Title: Threshold-free Attribute Profile for Classification of Hyperspectral Images

This paper appears in: IEEE Transactions on Geoscience and Remote Sensing

Date of Publication: 2019

Author(s): Kaushal Bhardwaj, Swarnajyoti Patra, Lorenzo Bruzzone

Volume: -, Issue: -

Page(s): -

DOI: 10.1109/TGRS.2019.2916169

Threshold-free Attribute Profile for Classification of Hyperspectral Images

Kaushal Bhardwaj and Swarnajyoti Patra, *Member, IEEE* and Lorenzo Bruzzone, *Fellow, IEEE*

***Abstract*—Selection of threshold values to generate non-redundant filtered images in attribute profiles is an unresolved issue. This paper presents a novel filtering approach to the construction of attribute profiles that does not require the definition of any threshold value. The proposed approach creates a max-tree (or min-tree), traverse to the first encountered leaf node using depth first traversal and defines a leaf attribute function (LAF) to demonstrate the changes in attribute values from leaf to root node. The LAF is analyzed based on a novel criterion to automatically detect the node along the path that has a first significant difference in attribute value. All its descendant nodes are merged to it and the process is repeated for each unvisited leaf node to create the final filtered tree which is transformed back as a filtered image. The proposed approach can incorporate maximum spatial information by applying few filtering operations without the need to define any threshold value. This is of great importance in spectral-spatial classification applications. Moreover, since the proposed approach requires one depth first traversal to generate a filtered image, it is very efficient in terms of computation time. To show the effectiveness of the proposed method, three real hyperspectral data sets are considered and the results are compared to a state-of-the-art method considering five different attributes. Results show that the proposed method has several important advantages with respect to the existing threshold based filtering techniques. Furthermore, the proposed method is also effective when compared with different spectral-spatial classification techniques.**

***Index Terms*—Hyperspectral images, classification, attribute filters, mathematical morphology.**

I. Introduction

Hyperspectral sensors acquire reflected light intensity from the considered scene in hundreds of contiguous bands [1]. The bands may range from the visible through the near and middle infrared to the thermal infrared portions of the spectrum [2]. Because of the rich spectral content, hyperspectral images (HSI), if properly analyzed, can provide better classification accuracies and recognize more detailed land-cover classes than multispectral images [3]. Moreover, pixels in either images are spatially correlated due to the homogeneous spatial distribution of land covers. Thus, information captured in neighboring locations provides useful supplementary knowledge for the analysis of a pixel. Therefore, spatial information along with the spectral features can effectively reduce the uncertainty of class assignment and shows further improvement in the classification results [4]. Several methods exist in the literature for spectral-spatial classification of HSI. A family of methods based on random fields and probabilistic graphs are developed in the framework of the Markov Random Fields (MRFs) theory. These methods provide a flexible spatial information modeling in image analysis which has been extensively applied to HSI data [5]. Another family of methods are based on sparse representation (SR). The pixelwise SR-based classification (SRC) techniques produce noisy classification maps [6]. To improve SRC, spectral and neighbouring information are jointly used with a fixed region based model (JSRC) [6] or a shape adaptive sparse model (SAS) [7]. To improve the SAS, a multi-scale adaptive SR (MASR) is proposed in [8]. Another method that combines unmixing and SR (USRC) is presented in [9]. All these SR-based methods are computationally demanding as they analyze each individual pixel of an HSI. To overcome this limitation, in [10] the HSI is segmented into superpixels and the whole superpixels are classified using a discriminative sparse model (SBSDM). Deep convolutional neural networks (CNN) based methods also have shown their potentiality for spectral-spatial classification of HSI in many recent papers [11]–[13]. A detailed survey of recent spectral-spatial classification techniques is presented in [5].

An interesting yet challenging way of integrating spectral and spatial information for HSI classification is based on mathematical morphology (MM) [14]. In the MM framework a wide range of morphological filters are available to incorporate spatial information. These are generally based on a fixed shape structuring element (SE) that decides the boundary of the neighborhood for a pixel [15], [16]. By varying the shape and the size of the SE, multiple filtering results can be obtained and concatenated with original images to form a morphological profile (MP) [14], [17], [18]. The SE-based morphological filters have the limitations that they are having a fixed shape structuring elements and are not able to filter the image based on gray level properties of the objects [19]. These limitations can be overcome by the attribute filters (AFs) [20], [21]. AFs are adaptive to the shape of the object and can filter the image using different properties (attributes) of objects based on the considered threshold value [22]. For a given gray-scale image, multiple filtered images are obtained using a sequence of threshold values. These images are concatenated with the original image to form an attribute profile (AP) [19]. In the literature, several works have exploited APs for classification purposes [23]–[27]. For HSIs, an extended attribute profile (EAP) can be constructed [28]. To construct the EAP, first the dimension of the HSI is reduced to few components by applying either a supervised or an unsupervised technique.

K. Bhardwaj and S. Patra are with the Department of Computer Science and Engineering, Tezpur University, 784028 Tezpur, India (e-mail: kauscsp@tezu.ernet.in; swpatra@tezu.ernet.in).

L. Bruzzone is with the Department of Information Engineering and Computer Science, University of Trento, Via Sommarive 14, I-38123 Trento, Italy (e-mail:lorenzo.bruzzone@ing.unitn.it).

Then, for each reduced component image, an AP is constructed and concatenated together [4], [29], [30]. A survey of spectral-spatial classification techniques based on APs is presented in [5], [31].

As explained above, an EAP is constructed by considering a single attribute that may not be sufficient to capture the full spatial information. To incorporate the variety of spatial information present in the images, multiple EAPs are constructed considering different attributes (for each EAP the threshold values are sampled manually from a wide range in small intervals) and are concatenated to form an extended multi attribute profile (EMAP) [4]. Such EMAP has a large dimensionality with a high redundancy, which affects the HSI classification in terms of curse of dimensionality problem [32]. In the literature this issue is addressed by reducing the dimensionality of the constructed EMAP using feature-selection techniques. In [33], a supervised feature-selection technique is presented to select an optimal subset of filtered images from the constructed EMAP for HSI classification. An unsupervised technique has been recently presented in [4] for the selection of the subset of filtered images. A drawback of such kind of approaches is that the construction of very large profiles considering a large number of threshold values may be a time consuming task.

An alternative approach to attribute profile based spectral-spatial HSI classification is the construction of a reduced profile [34]. In this approach an extended reduced AP (ErAP) corresponding to an HSI is constructed, which has lower dimensionality with similar discriminating capability as compared to EAP. To construct such ErAP, first the dimension of the HSI is reduced and then for each gray-scale image in the reduced domain a reduced AP (rAP) is constructed and concatenated together. In [34], to construct the rAP for a given image its thinning and thickening profiles are generated considering a set of manually selected threshold values. Then separate differential attribute profiles (DAP) are generated corresponding to thinning and thickening profiles. After that, for each DAP a component hierarchy is constructed and the most homogeneous connected component is chosen from each path of the hierarchy to construct a segmented image. Finally, a rAP is constructed consisting of three images: the original image and two segmented images (one obtained from the thickening profile and the other one from the thinning profile). This approach avoids the curse of dimensionality problem by constructing a smaller profile. However, a drawback of this approach is the variation in the results due to the quality of segmented images included in the rAP, which is dependent on the manually selected threshold values used to generate the thickening and thinning profiles. Also the approach has the overhead of creating DAPs and component hierarchy.

All the aforementioned methods construct the profiles based on manually selected threshold values. In the literature, few works address the problem of constructing attribute profiles by selecting the threshold values automatically [30], [35], [36]. The first approach in this direction was presented in [35], where a preliminary clustering or classification is performed on an image and the attribute values obtained for different connected components of the resultant image are included in a vector which is again clustered to obtain the final set of threshold values. This approach is sensitive to the results of preliminary classification. Cavallaro *et. al.* have presented an interesting method where threshold values are identified and the profile is created in fully automatic way [37]. A drawback of this method is that it is computationally demanding.

The attribute profile based spectral-spatial classification methods existing in the literature require the definition of the threshold values either manually or automatically for generating the filtered images. Since a single filtered image is unable to capture sufficient spatial information, multiple threshold values are used to generate several filtered images in an attribute profile. As a result, the construction of an attribute profile is time consuming and may result in a high dimensionality. To the best of our knowledge, no method has been proposed in the HSI literature that generates attribute profiles without employing threshold values. In this paper, we propose a novel approach to construct attribute profiles without considering threshold values. In our approach, a small number of filtered images are generated, which are able to capture the maximum spatial information by analyzing the connected components of the considered image. To this end, first a max-tree (or min-tree) of the image is created, where the nodes of the tree represent different connected components of the image. Then, the tree is pruned in a way such that all the leaf nodes of the pruned tree represent significant objects of the image. In our method, first, by applying a depth first traversal a leaf node is reached. Then a leaf attribute function (LAF) is defined to compute the attribute value of each node in the path. After that, starting from the leaf node, all the nodes in the path are analyzed using LAF and the first node in the path that has a significant difference in the attribute values is automatically recognized. Finally, all the descendant nodes of the recognized node are merged to it for pruning. This process is repeated for all the paths obtained for the remaining unvisited leaf nodes to get the final filtered tree, which is transformed back to a gray-scale image. The advantages of the proposed filtering method are as follows: (i) It generates the filtered images without using any threshold value; (ii) It is fully automatic and independent on the image content; (iii) The small number of filtered images generated are able to capture sufficient spatial information; (iv) It avoids the curse of dimensionality problem as the profile constructed has relatively low dimension; and (v) It is computationally efficient when compared to the conventional threshold based filtering methods.

The rest of the paper is organized as follows. Section II describes the attribute filters and the construction of attribute profiles recalling the main concepts presented in the literature. Section III presents the proposed threshold-free attribute filter and the construction of the attribute profile as well as the extended attribute profile. The experimental results on three real hyperspectral data sets are illustrated and discussed in Section IV. Finally, Section V concludes the paper also addressing some future developments.

II. Attribute Profiles

Attribute profiles fuse spectral and spatial information by concatenating a given image with its attribute filtering results

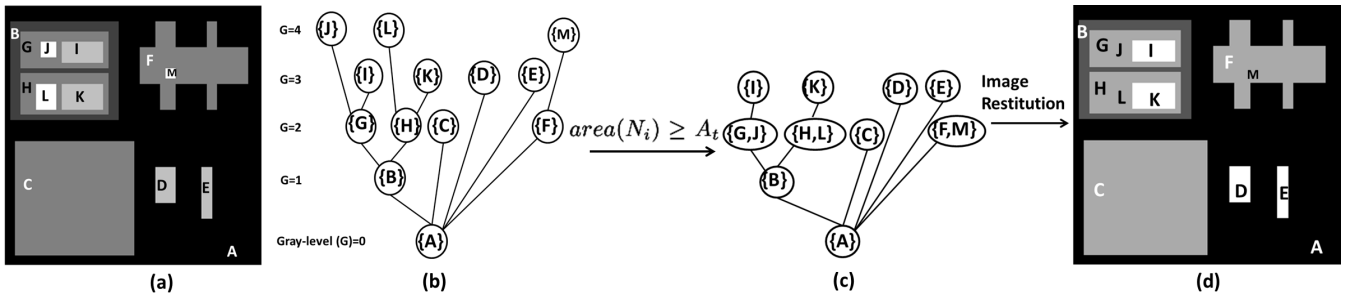

Fig. 1. Attribute filtering of a simple gray-scale image. (a) Original gray-scale image, (b) max-tree corresponding to the gray-scale image, (c) Filtered max-tree using attribute *area* and threshold value A_t, (d) Filtered image after restitution from the filtered max-tree.

[19]. They are generated based on three phases, namely max-tree (min-tree) creation, filtering of the max-tree (min-tree) and image restitution [22]. The details of each of the phase are explained below.

1) Phase 1 – Max-tree (min-tree) creation: Since attribute filtering is based on a tree representation of the image, we need to create a tree corresponding to the given image. To this end several tree representations of images are available [38], [39]. Among them, max-tree (min-tree) is a widely accepted choice in literature [22], [28], [33], [34], [37], [40]. In a max-tree (min-tree), the pixels with minimum (maximum) gray-values are assigned to the root and pixels with higher (lower) gray-values are assigned to child nodes corresponding to the nested connected components. An example of max-tree is shown in Fig. 1(b), where the root has pixels of background with gray-value zero. As one can see from the figure, the connected components are the nodes of the tree and links between the nodes represent the parent-child relationship between nested connected components.

2) Phase 2 – Max-tree (min-tree) filtering: The nodes of the constructed max-tree (min-tree) represent connected components in the image and possess computable properties (also called attributes). Example of these attributes are *area*, *diagonal of bounding box*, *area of bounding box*, *perimeter*, *etc*. These attributes are used to define a criterion which is ultimately used for pruning the tree. The criterion is defined as a logical condition based on attribute threshold values. For example, let the attribute be *area* and the threshold value be A_t. A criterion can be $area(N_i) \geq A_t$ (*area* at N_i is greater than the given threshold value A_t), where N_i represents a node of the max-tree (min-tree). The defined criterion is evaluated at each node of the tree and the nodes that do not satisfy the criterion are merged to their parent. An example of a filtered max-tree is shown in Fig. 1(c), where the considered attribute and threshold values for filtering are *area* and A_t, respectively. Let us assume that the nodes J, L and M have an *area* value smaller than A_t. Then, they are merged to their parents G, H and F, respectively, during the filtering operation. Merging is the process of assigning the pixels at a given node to their parent node so that the pixels could be represented by the same gray-value as of the parent.

3) Phase 3 – Image restitution: Once the max-tree (min-tree) has been filtered, the filtered max-tree (min-tree) is transformed back to a gray-scale image by assigning to each pixel the gray-level of its corresponding node in the max-tree (min-tree) as shown in Figure 1(d).

After passing through these three phases, one can get a filtered image. This three-phase operation on an image using max-tree (min-tree) is called *attribute thinning* (*attribute thickening*). An attribute thinning profile (ThP) is constructed by applying the thinning operation to a gray-scale image using multiple threshold values [19]. It can be defined as:

$$ThP(I) = \left\{\gamma^{\lambda_1}(I), \gamma^{\lambda_2}(I), ..., \gamma^{\lambda_T}(I)\right\} \tag{1}$$

where $\gamma^{\lambda_i}(I)$ represents the thinning operation on the image I using λ_i ($\lambda_i < \lambda_{i+1}$) as filtering threshold value. Multiple thickening operations on the given image I will result in an attribute thickening profile (TkP) [19], which can be defined as:

$$TkP(I) = \left\{\Phi^{\lambda_1}(I), \Phi^{\lambda_2}(I), ..., \Phi^{\lambda_T}(I)\right\} \tag{2}$$

where $\Phi^{\lambda_i}(I)$ is the attribute thickening operation on image I using the threshold value λ_i. The attribute profile for a given gray-scale image I is constructed by concatenation of the image I with its thinning and thickening profiles [19].

$$AP(I) = \{TkP(I),\ I,\ ThP(I)\} \tag{3}$$

III. Proposed Threshold-free Attribute Profile

With the aim to filter a given image without using any threshold value and to incorporate maximum spatial information, the following Subsections present a novel threshold-free attribute filter approach to the construction of spectral-spatial profiles.

A. Threshold-free Attribute Filter

The primary focus of this paper is to develop a novel approach such that the filtering step becomes threshold-free. Note that in our work the max-tree (min-tree) creation and the image restitution steps are exactly the same as in the literature techniques. In the proposed filtering method, the tree that represents the image is traversed to a leaf node and the attribute values of the nodes in the path are analyzed to detect the first node (in the direction from leaf towards root) with a significant difference in the attribute value. The detected node is marked and all its descendant nodes are merged to it. Repeating this for the remaining leaf nodes leads to filtering few insignificant objects from each connected component of the given image

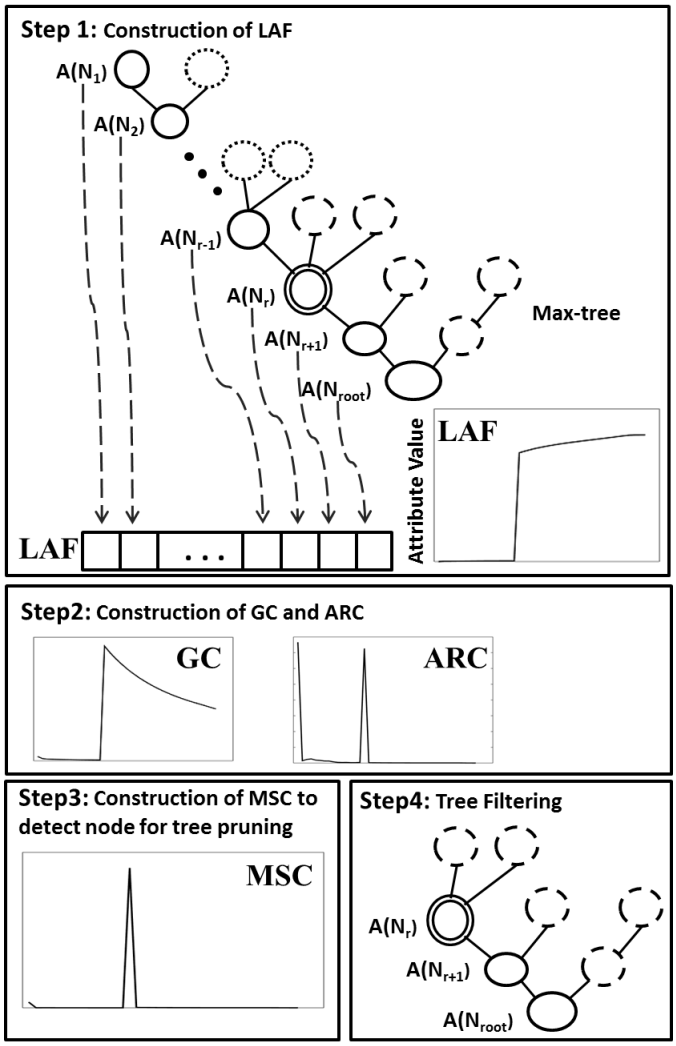

Fig. 2. Steps of the proposed threshold-free attribute filtering technique considering a path from a leaf node to the root node obtained by applying depth first traversal.

irrespectively of their shape and size. The traversal of the tree should be depth first for two reasons. Firstly, it helps in keeping track of the followed path. Secondly, it suppresses the possibility of visiting a pre-visited node which ultimately helps in completing the filtering process in one traversal. The filtering process considering the path to a leaf node of the max-tree is demonstrated in Fig. 2. The nodes N_i on the path from leaf to root are in bold circles and their corresponding attribute values A(N_i) are shown to the left of each node. The node N_r where the first significant change in attribute values occurred is shown with a double concentric circle. The nodes in dotted circles are children of the nodes in the path between the leaf N_1 and the node N_r. On filtering, these dotted nodes are also merged to N_r along with the nodes on the path. The dashed circles represent the subtree of the nodes between N_r and the root which must remain untouched while current filtering operation. As one can see from the figure, the proposed filtering procedure starts with the construction of a leaf attribute function (LAF) pooling the attribute values of the nodes on the path. In the second step, the LAF is analyzed to construct two curves namely, gradient curve (GC), which shows significant differences, and attribute ratio curve (ARC), which determines sudden changes in the attribute value. In the third step, the GC and ARC are combined to construct maximal suitability curve (MSC) from which a node is automatically detected (N_r in our example) to prune the tree. In the last step, the tree is pruned from the detected node and all the nodes between N_1 and N_{R-1} (including N_1 and N_{R-1}) along with their children (identified in dotted circles) are merged to N_R maintaining the consistency in the number and membership of pixels. The proposed four-steps procedure is repeated for each unvisited leaf node of the updated tree to get the final filtered tree, which is then transformed back to a gray-scale image. The details of these four steps of the proposed attribute filter are described below.

1) Step 1 – Construction of LAF: This paper introduces the leaf attribute function (LAF) that computes the attribute values of each node on the considered path from the leaf to root node. The LAF can be analyzed to see the changes in attribute values from leaf towards root. Note that in a max-tree every leaf node has exactly one path. Given that there are P nodes in the path starting from the leaf node N_ℓ to the root, the LAF for the leaf node N_ℓ is defined as:

$$LAF_{N_\ell}(i) = A(N_i), \qquad i = 1, 2, ..., P. \tag{4}$$

where N_i is the i^{th} node on the path starting from the leaf node and $A(N_i)$ is the attribute value of a node N_i considering all the pixels associated to it and its descendant nodes. The LAF for a leaf node N_ℓ is constructed while traversing the tree to the leaf node N_ℓ adopting depth first traversal. Once we reach the leaf node, the LAF corresponding to N_ℓ is generated and is ready for analysis.

2) Step 2 – Construction of GC and ARC: The LAF for a leaf node can be seen as an array which contains the attribute values of every node on the path starting from the leaf to the root. Fig. 3(a) shows few LAFs for randomly selected leaf nodes of a max-tree constructed from the first principal component (PC) of the University of Pavia data set (see Section IV) considering *area* as attribute. From the figure one can see that LAF is an increasing function and starting from the leaf node the attribute values are increasing smoothly. After few nodes there is a sudden exponential increment in the attribute values. The node which is responsible for such sudden increment in attribute values is considered as a node for representing the first significant object in the path. The goal of the filtering procedure is to automatically detect such nodes for all the paths in the tree. For this purpose the proposed method generated two curves namely, gradient curve (GC) and attribute ratio curve (ARC) by analyzing the LAF.

Gradient Curve (GC): To detect the suitable node on the considered path that is associated with the first significant difference in attribute values, we compute the gradient from the leaf's plotted position on the LAF curve (i.e., the starting point of the curve) to each of the break points on it. Please note that the break points on the LAF curve represent the corresponding attribute values for the intermediate nodes of the considered path. Fig. 4 shows an LAF curve where the dotted

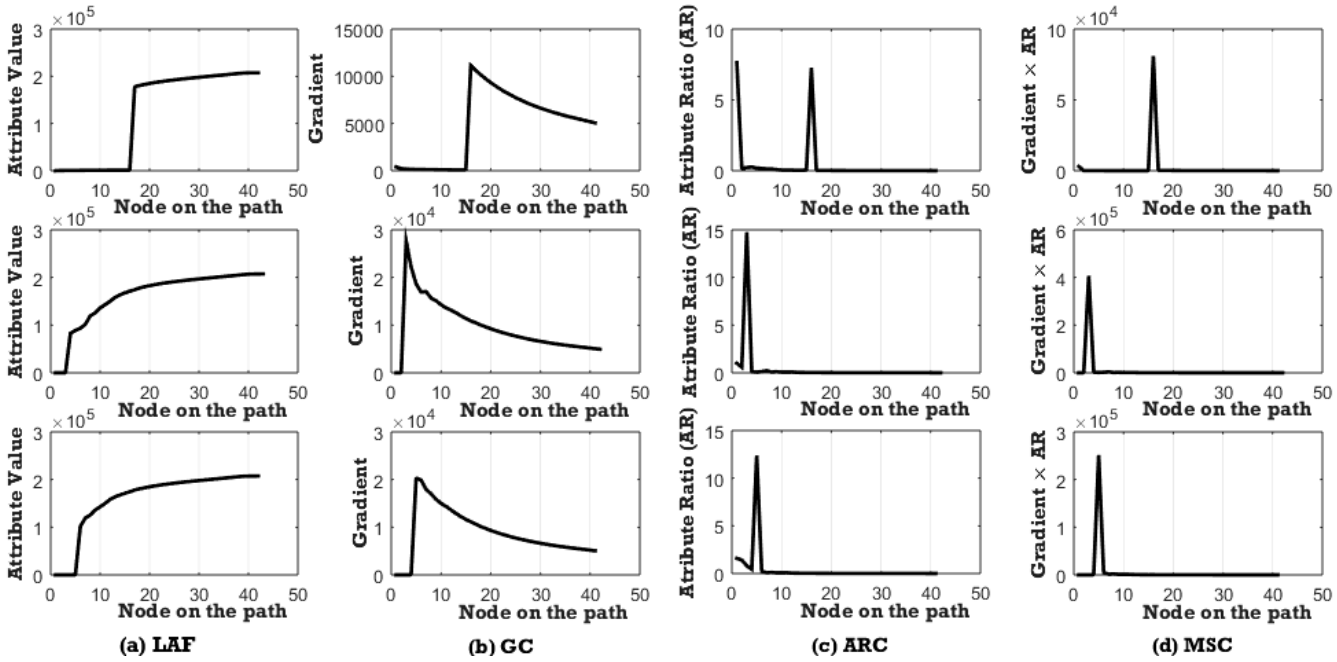

Fig. 3. (a) Leaf attribute functions (LAF); (b) gradient curves (GC); (c) attribute ratio curves (ARC); and (d) maximal suitability curves (MSC) obtained by analyzing three randomly selected paths from the max-tree. Each path is obtained from a randomly selected leaf node to the root node of the max-tree created by considering 1^{st} PC of University of Pavia data set.

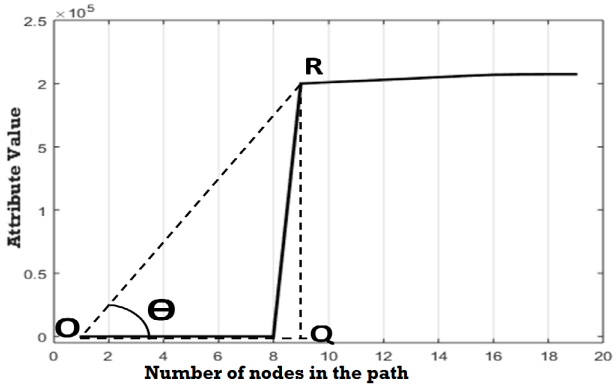

Fig. 4. An LAF representing the attribute values in the path from a randomly selected leaf node to the root. O is the starting position and R is the position on LAF having maximum gradient from O.

lines help us in understanding the computation of gradient for a break point from the starting position of the curve. The gradient $tan(\theta)$ from the starting point O to a break point R can be computed as:

$$Gradient(OR) = \frac{RQ}{OQ} = \frac{LAF_{N_\ell}(i) - LAF_{N_\ell}(1)}{i-1} \quad (5)$$

where i is the position of a node on the path from N_ℓ to the root such that $A(N_i) = R$. A GC is created by calculating the gradient for each node on the path and is formally defined as follows:

$$GC_{N_\ell}(i) = \left\{ \frac{LAF_{N_\ell}(i+1) - LAF_{N_\ell}(1)}{i} \right\}, \; i = 1, 2, ..., P-1. \quad (6)$$

Fig. 3(b) shows some gradient curves corresponding to the LAFs illustrated in Fig. 3(a). From these figures one can see that initially the gradient has an increasing behavior by increasing the attribute value and reaches the maximum at the node which has first significant difference in attribute value. After that, the LAF keeps increasing trend whereas the gradient starts to decrease.

Attribute Ratio Curve (ARC): To detect the node that is associated with a sudden change in the attribute values on the considered path, we propose to compute the ratio between the attribute value of a node and the attribute value of its child node on the considered path. The ARC for a path associated to the leaf node N_ℓ can be computed as:

$$ARC_{N_\ell}(i) = \log_2 \left(\frac{LAF_{N_\ell}(i+1)}{LAF_{N_\ell}(i)} \right), \quad i = 1, 2, ..., P-1. \quad (7)$$

where i is the node number from the leaf to root and P is the total number of nodes on the considered path. Fig. 3(c) shows few ARCs corresponding to the LAFs shown in Fig. 3(a). From these figures one can see that an ARC has a local maximum at the node that is associated with sudden changes in attribute values. Hence, ARC can be used to detect a node on the considered path which is responsible for such sudden changes in attribute values.

3) Step 3 – Construction of MSC to detect node for tree pruning: To detect the first node (starting from the leaf node on the considered path) that represents a significant object in the image, a maximal suitability curve (MSC) is generated by combining GC and ARC. The MSC for the leaf node N_ℓ can be defined as:

$$MSC_{N_\ell}(i) = GC_{N_\ell}(i) \cdot ARC_{N_\ell}(i), \quad i = 1, 2, ..., P-1. \quad (8)$$

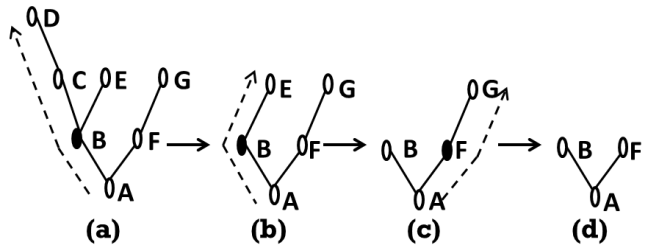

Fig. 5. A synthetic tree and the filtered trees obtained by the proposed technique after detecting a node (represented with filled circle) from the path (b) A to D (c) A to E and (d) A to G..

which can be written as:

$$MSC_{N_\ell}(i) = \left(\frac{LAF_{N_\ell}(i+1) - LAF_{N_\ell}(1)}{i}\right) \cdot \log_2\left(\frac{LAF_{N_\ell}(i+1)}{LAF_{N_\ell}(i)}\right) \tag{9}$$

From the above equation one can see that the MSC provides high values when both GC and ARC have high values. Fig. 3(d) shows few maximal suitability curves corresponding to the LAFs shown in Fig. 3(a). In our work the node on the considered path that is associated with the global maxima of MSC is recognized as the node that represents a significant object in the image.

4) Step 4 – Tree filtering: Once the node is detected on the path, all its descendants are merged to it for pruning. Merging means that all the pixels associated to the descendants are assigned to the detected node. This is similar to the min strategy used for filtering [22]. In greater detail, Fig. 5 demonstrates the proposed tree filtering technique by considering the synthetic tree shown in Fig. 5(a). First, a path from root node A to leaf node D (shown by the dashed line in Fig. 5(a)) is obtained for analysis by using depth first traversal. From the path, if we assume that the node B is detected by our proposed technique for merging, then all the descendant nodes of B will be merged to it and the obtained resultant tree is shown in Fig. 5 (b). Now resuming the depth first traversal from B, a path from A to leaf node E (shown by the dashed line in Fig. 5(b)) is obtained for analysis. For this path, if B is the suitable node detected by our technique, then after merging we get the tree shown in Fig. 5(c). Resuming the depth first traversal from B, a path from A to leaf node G (shown by the dashed line in Fig. 5(c)) is obtained for analysis. For this path, if we assume F is the suitable node detected by the proposed technique, then the resultant tree obtained after merging its descendants is that presented in Fig. 5(d). Since at this point all the leaf nodes of the original tree are processed, the algorithm will stop and the resultant tree is considered as filtered tree. The filtered tree is restituted back to a gray-scale image where all the connected components of the given image have been filtered automatically. For restitution, the same procedure is used as explained in Subsection II-3. The proposed filtering technique is increasing, anti extensive and non idempotent in nature. The steps of the proposed attribute filtering method are shown in Algorithm 1.

Algorithm 1 Proposed attribute filtering technique

Input: The gray-scale image I,
Attribute A (*area*, *perimeter*, *etc*.)
Output: The filtered Image I'.

1: Create a max-tree T for image I.
2: Traverse the tree T using depth first traversal and reach the first leaf node.
3: **repeat**
4: Analyze the attribute values of all the nodes in the path starting from the leaf node and define a LAF using (4).
5: Create a gradient curve (GC) based on LAF using (6).
6: Create an attribute ratio curve (ARC) based on LAF using (7).
7: Combine the GC and ARC to generate maximal suitability curve (MSC) as defined in (8).
8: Detect the node associated to the global maximum of the MSC and merge all its descendant nodes to it.
9: Resume the depth first traversal from the detected node towards the next leaf node.
10: **until** All the leaf nodes of the tree T are visited.
11: Transform the filtered tree to the gray-scale image I'

B. Construction of Threshold-free Attribute Profile

So far, we discussed a threshold-free attribute filtering technique that works on a gray-scale image using max-tree. Such filtering of an image is called attribute thinning operation and it filters out bright objects. If the proposed automatic filtering procedure is applied again to the resultant max-tree obtained after the first filtering, the next group of connected components can be filtered out from the given image. Therefore, a set of filtered images can be generated by applying the proposed automatic filtering procedure to the resultant filtered max-trees. Such set of filtered images constructed using the max-tree of the given image can be stacked together to form a thinning profile (ThP). The ThP for a gray-scale image I considering the proposed thinning operation can be defined as

$$ThP(I) = \left\{\gamma^1(I), \gamma^2(I), ..., \gamma^T(I)\right\} \tag{10}$$

where $\gamma^i(I)$ represents the i^{th} threshold-free thinning operation on the image I. $\gamma^i(I)$ is obtained by applying the proposed automatic filtering procedure to the resultant max-tree of $\gamma^{i-1}(I)$. The proposed filtering is done using the min-tree created for the same image to filter dark objects and is called attribute thickening operation. Multiple filtering operations on the min-tree constructed for the given image I will result in thickening profile (TkP), which can be defined as

$$TkP(I) = \left\{\Phi^1(I), \Phi^2(I), ..., \Phi^T(I)\right\} \tag{11}$$

where $\Phi^i(I)$ represents the i^{th} threshold-free thickening operation on the image I. $\Phi^i(I)$ is obtained by applying the proposed automatic filtering to the resultant min-tree of $\Phi^{i-1}(I)$. The value T represents the number of filtering operations. An attribute profile (AP) is a concatenation of the original image with its thickening and thinning profiles as defined in (3).

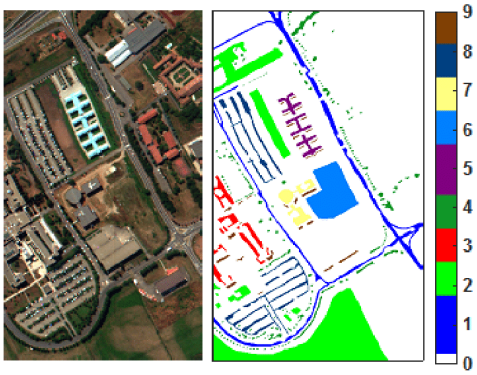

Fig. 6. Three band color image of the ROSIS University of Pavia data set and its related map of available reference samples.

Considering an hyperspectral image H, an extended attribute profile (EAP) is constructed by concatenating the AP constructed for each gray-scale image in a reduced subset derived from the original channels, which can be defined as

$$EAP(I) = \{AP(PC_1),\ AP(PC_2), ...,\ AP(PC_p)\} \quad (12)$$

where PC_i is the i^{th} principal component (PC) extracted from HSI in order to reduce its dimension and p is the number of considered PCs. p can be selected on the basis of the information content present in the first components (e.g. considering the first PCs that contain 99% of the total information).

IV. Experimental results

A. Data Set Description

The effectiveness of proposed method is assessed using three different hyperspectral data sets. The First data set[1] is an HSI acquired by the ROSIS-03 (Reflective Optics System Imaging Spectrometer) airborne optical sensor over the urban area of the University of Pavia, Italy. The ROSIS-03 sensor acquires images in 115 data channels with a spectral coverage ranging from 430 to 860 nm. Twelve channels have been removed due to noise and the remaining 103 spectral bands are processed. The size of the image in pixels is 610×340, with a spatial resolution of 1.3 m. Fig. 6 shows a false color composite of the image and a map of available reference samples.

The second data set[2] is another benchmark HSI acquired by the AVIRIS sensor over the agricultural land of Indian Pines, Indiana, in the early growing season of 1992. The image consists of 145×145 pixels with a spatial resolution of 20 m. The acquired image has 220 data channels with a spectral coverage ranging from 400 to 2500 nm, with a spectral resolution of about 10 nm. Twenty water absorption and fifteen noisy bands were removed and the remaining 185 bands were considered in experiments. Fig. 7 shows a false color composition and a map of the available reference samples for the AVIRIS Indian Pines scene.

[1]Available online:http://www.ehu.eus/ccwintco/index.php?title=Hyperspectral_Remote_Sensing_Scenes

[2]Available online: http://engineering.purdue.edu/ biehl/MultiSpec

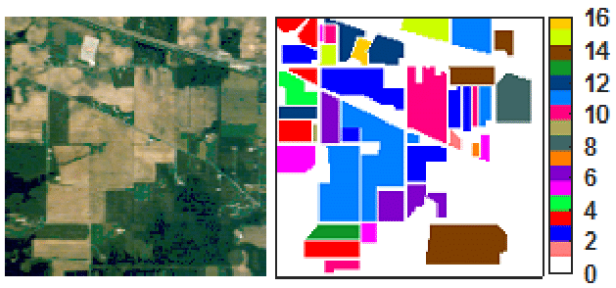

Fig. 7. Three band color image of the AVIRIS Indian Pines data set and its related map of available reference samples.

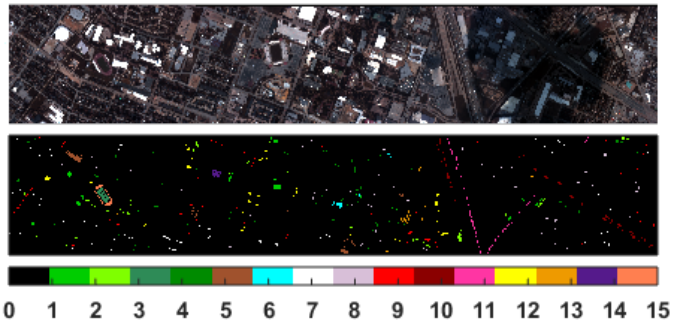

Fig. 8. Three band color image of the CASI University of Houston data set and its related map of available reference samples.

The third data set[3] is an HSI acquired over the campus of University of Houston, Texas, United States and its neighboring urban area by the Compact Airborne Spectro-graphic Imager (CASI). The size of the image is 349×1905 pixels with a spatial resolution of 2.5 m. The image has 144 spectral bands covering a range from 380 to 1050 nm. Fig. 8 shows a false composition of the considered image and a map of the available reference samples.

B. Design of Experiments

In order to validate the effectiveness of proposed method the experimental analysis is carried out on the three aforementioned hyperspectral data sets. For each data set, spectral-spatial profiles are created using the proposed method and the state-of-the-art method considering five attributes namely *area*, *perimeter*, *area of bounding box (Abb)*, *diagonal of bounding box (Dbb)* and *standard deviation (Std)*. Among these, *area*, *Abb* and *Dbb* are increasing attributes, whereas *perimeter* and *Std* are non-increasing attributes. The dimension of the hyperspectral feature space is reduced by considering the first five principal components which preserve almost 99% of the original HSIs information. The dimensionality of the profile constructed by the proposed method (referred as $EAP_{proposed}$ hereafter) depends on the number of times (T) the filtering operation is performed. The experiments are carried out with three different settings, $T = 1$, $T = 2$ and $T = 3$. The dimensions of the $EAP_{proposed}$ for first five PCs considering $T = 1$, $T = 2$ and $T = 3$ are 15, 25 and 35, respectively. The proposed method is compared to the very recent and effective

[3]Available online: http://hyperspectral.ee.uh.edu/?page˙id=459

TABLE I
CLASSIFICATION RESULTS OBTAINED FOR PROFILES CONSTRUCTED BY THE PROPOSED AND THE STATE-OF-THE-ART METHODS CONSIDERING FIVE DIFFERENT ATTRIBUTES (UNIVERSITY OF PAVIA). THE BEST VALUES ARE HIGHLIGHTED IN BOLD FACE

		$EAP_{Num\_regions}$			EAP_{Num_pixel}			EAP_{Sum_gray}			$EAP_{proposed}$		
#features		15	25	35	15	25	35	15	25	35	15	25	35
Area	$\overline{OA}$	87.012	89.550	92.544	93.125	99.319	99.327	90.017	98.851	99.395	**98.818**	**99.519**	**99.632**
	kappa	0.8243	0.8595	0.9006	0.9084	0.9910	0.9911	0.8660	0.9848	0.9920	**0.9843**	**0.9936**	**0.9951**
	std	0.0721	0.1215	0.1121	0.0896	0.0539	0.0510	0.1325	0.0752	**0.0360**	**0.0561**	**0.0408**	0.0441
Perimeter	$\overline{OA}$	87.259	89.388	92.726	89.217	93.777	98.929	88.750	93.292	98.590	**98.937**	**99.418**	**99.496**
	kappa	0.8278	0.8573	0.9030	0.8550	0.9172	0.9858	0.8484	0.9107	0.9813	**0.9859**	**0.9923**	**0.9933**
	std	0.1336	0.1538	0.0634	0.1359	0.1095	**0.0394**	0.1344	0.0712	0.0504	**0.0608**	**0.0380**	0.0486
Abb	$\overline{OA}$	86.891	89.041	91.642	89.286	97.319	99.555	88.643	96.095	99.415	**98.628**	**99.315**	**99.600**
	kappa	0.8226	0.8525	0.8882	0.8559	0.9644	0.9941	0.8471	0.9482	0.9922	**0.9818**	**0.9909**	**0.9947**
	std	0.1685	0.1160	0.0800	0.1538	0.0516	0.0529	0.1742	0.1096	0.0659	**0.0800**	**0.0406**	**0.0481**
Dbb	$\overline{OA}$	86.807	88.883	91.421	89.261	96.718	99.545	88.668	95.016	99.310	**97.751**	**99.019**	**99.673**
	kappa	0.8216	0.8503	0.8852	0.8556	0.9564	0.9940	0.8475	0.9338	0.9908	**0.9701**	**0.9870**	**0.9957**
	std	0.0904	0.1037	0.0878	0.1306	0.0942	0.0333	0.2022	0.1086	**0.0279**	**0.0732**	**0.0734**	0.0599
Std	$\overline{OA}$	86.878	88.984	91.644	**89.292**	**97.289**	**99.567**	88.668	96.057	99.358	88.280	95.176	98.074
	kappa	0.8225	0.8518	0.8882	**0.8559**	**0.9640**	**0.9943**	0.8474	0.9476	0.9915	0.8421	0.9358	0.9745
	std	0.1657	0.1569	0.1111	**0.0773**	0.0820	**0.0396**	0.0892	**0.0602**	0.0562	0.1421	0.0785	0.0963

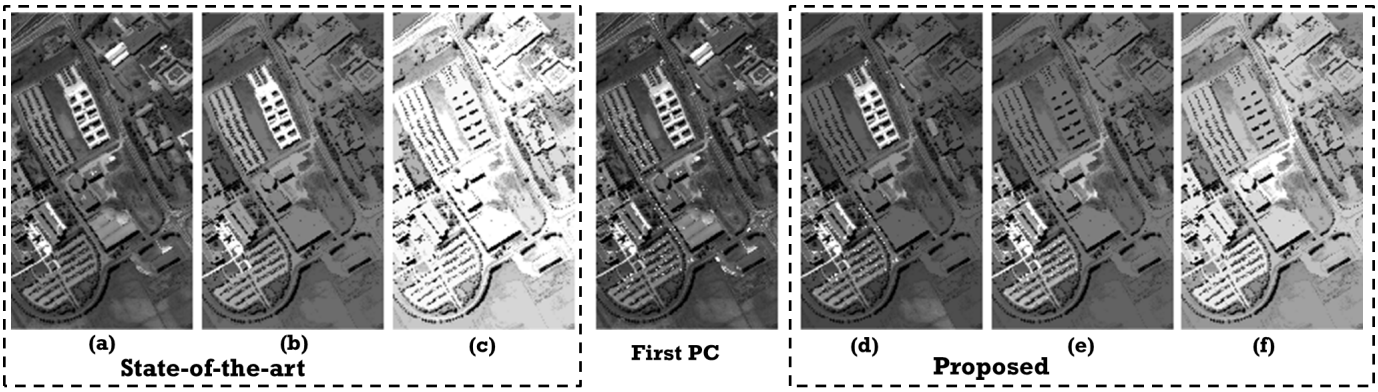

Fig. 9. Filtered images obtained by applying the state-of-the-art and the proposed filtering method to the 1^{st} principal component of the University of Pavia data set by considering the *area of bounding box* attribute. The best filtered image obtained by the state-of-the-art method [37] considering (a) the 1^{st} threshold, (b) the 2^{nd} threshold and (c) the 3^{rd} threshold. The filtered image obtained by the proposed method after applying (d) the 1^{st}, (e) the 2^{nd} and (f) the 3^{rd} filtering operation.

state-of-the-art method presented in [37], which creates EAP using a set of automatically detected threshold values. For the detection of such thresholds, the method first exploits the tree structure and generates a large number of threshold values automatically. Then, a vector called GCF is created that stores a measure computed corresponding to each threshold value. The measures used in [37] are *number of changed regions*, *number of changed pixels* and *sum of gray-level values*. The created GCF is approximated using regression and break points of the approximated curve are referred as final detected threshold values. Finally, considering the same PCs as used by our method, the EAP is constructed by applying the automatically detected threshold values.

The spectral-spatial profiles constructed by the state-of-the-art method considering the *number of changed regions*, the *number of changed pixels* and the *sum of gray-level values* are referred in this paper as $EAP_{Num\_regions}$, EAP_{Num_pixel} and EAP_{Sum_gray}, respectively. For a fair comparison, these profiles are also constructed with the same number of features (images) as those of the $EAP_{proposed}$. A one-against-all support vector machine (SVM) classifier with radial-basis-function (RBF) kernel is used for classification purposes. The SVM parameters are obtained by performing grid search with 5-fold cross-validation. In the experiments, ten separate pairs of the training and test sets are generated, each of which is composed of a training set having 30% of the labeled samples randomly selected from each class and a test set having the rest 70% of the samples. The classification results are reported in terms of average overall accuracy ($\overline{OA}$), the related standard deviation (std) and the average kappa accuracy (kappa). All the algorithms are implemented in MATLAB (R2015a) and the SVM classifier is implemented using the LIBSVM library [41]. However, note that any classifier can be used for classifying the constructed attribute profiles, which are general and classifier independent. The regression is implemented using the code available in [42].

C. Results

To evaluate the effectiveness of the attribute profiles constructed by the proposed method ($EAP_{proposed}$), the first experimental analysis is carried out on the University of Pavia data set. Table I reports the classification results obtained for the $EAP_{proposed}$, the $EAP_{Num\_regions}$, the EAP_{Num_pixel} and the EAP_{Sum_gray} considering five different attributes

TABLE II
CLASSIFICATION RESULTS OBTAINED FOR PROFILES CONSTRUCTED BY THE PROPOSED AND THE STATE-OF-THE-ART METHODS CONSIDERING FIVE DIFFERENT ATTRIBUTES (INDIAN PINES). THE BEST VALUES ARE HIGHLIGHTED IN BOLD FACE

		$EAP_{Num\_regions}$			EAP_{Num_pixel}			EAP_{Sum_gray}			$EAP_{proposed}$		
#features		15	25	35	15	25	35	15	25	35	15	25	35
Area	$\overline{OA}$	80.725	83.264	88.199	85.875	96.067	96.094	85.273	95.879	96.053	**95.399**	**96.431**	**96.731**
	kappa	0.7794	0.8086	0.8652	0.8387	0.9551	0.9554	0.8318	0.9530	0.9550	**0.9475**	**0.9593**	**0.9627**
	std	0.3090	0.4167	0.3118	0.3061	0.3345	**0.1752**	0.2952	**0.2162**	0.2458	**0.2871**	0.2576	0.2783
Perimeter	$\overline{OA}$	80.987	85.246	92.390	83.133	89.480	96.287	82.189	88.211	95.847	**95.139**	**96.370**	**96.548**
	kappa	0.7824	0.8313	0.9131	0.8072	0.8799	0.9576	0.7964	0.8654	0.9526	**0.9445**	**0.9586**	**0.9606**
	std	0.3784	0.4256	0.2360	0.2946	0.4039	0.1643	0.3720	0.3680	**0.1578**	**0.1443**	**0.3327**	0.2172
Abb	$\overline{OA}$	80.637	82.554	86.915	83.435	93.194	96.294	82.232	89.565	95.850	**95.036**	**96.229**	**96.675**
	kappa	0.7782	0.8005	0.8504	0.8107	0.9223	0.9577	0.7968	0.8809	0.9526	**0.9434**	**0.9570**	**0.9621**
	std	0.3847	0.2970	0.2939	0.3461	0.3764	0.3767	0.2348	0.2487	0.3283	**0.1978**	**0.2446**	**0.2449**
Dbb	$\overline{OA}$	80.797	82.204	87.191	82.725	93.252	96.243	81.780	89.197	95.918	**94.489**	**96.123**	**96.385**
	kappa	0.7802	0.7964	0.8536	0.8024	0.9230	0.9571	0.7916	0.8767	0.9534	**0.9371**	**0.9558**	**0.9588**
	std	**0.2418**	0.2918	0.4421	0.3038	0.2125	0.2322	0.4176	0.3815	**0.1848**	0.3364	**0.1759**	0.2401
Std	$\overline{OA}$	80.756	86.279	93.149	**92.579**	**94.957**	94.553	89.321	94.096	94.347	82.189	92.240	**95.827**
	kappa	0.7796	0.8433	0.9218	**0.9153**	**0.9425**	0.9378	0.8781	0.9326	0.9355	0.7963	0.9115	**0.9524**
	std	0.3528	0.4155	0.2944	**0.2975**	0.3020	0.3705	0.4293	0.3200	**0.2003**	0.3472	**0.1944**	0.2109

namely *area*, *perimeter*, *Abb*, *Dbb* and *Std*. From the table one can see that except *Std*, for the remaining attributes the $EAP_{proposed}$ with 15 features provided significantly higher average overall accuracies ($\overline{OA}$) than those obtained by all the three profiles of the same size constructed by the state-of-the-art method. As an example, for the *area* attribute, among the three profiles constructed by the state-of-the-art method the best $\overline{OA}$ (achieved by the EAP_{Sum_gray} with 35 features) is 99.39%. Whereas, the $EAP_{proposed}$ constructed by the proposed method with only 15 features provided an $\overline{OA}$ of 98.82% and with 25 features it provided 99.52%. For *Std* attribute, both the proposed and the state-of-the art methods produced similar results. One of the important advantages of the proposed method is that it incorporates maximum spatial information in the first filtering operation, which is confirmed by the results obtained for the $EAP_{proposed}$ with 15 features. The filtered images obtained for the first PC of the University of Pavia data set using the proposed filtering method (applying 1^{st}, 2^{nd} and 3^{rd} filtering operation) and the state-of-the-art method (applying 1^{st}, 2^{nd} and 3^{rd} threshold values detected by using the best measure) considering *area of bounding box* attributes are shown in Fig. 9. From the figure one can see that the state-of-the-art method was able to filter only a few objects by considering the 1^{st} detected threshold. Whereas, the proposed filtering method was able to filter more objects by applying 1^{st} filtering operation. This added a significant background information in a single filtering operation, which is of great importance in spectral-spatial classification problems.

For the Indian Pines data set, the classification results obtained by considering different attributes are shown in Table II. Also for this data set, one can see that the $EAP_{proposed}$ defined by the proposed technique outperformed the EAPs defined by the state-of-the-art method [37]. Considering all the increasing attributes and the non-increasing attribute *perimeter*, the lowest $\overline{OA}$ produced by the $EAP_{proposed}$ with 15 features is 94.48%. Whereas, the highest $\overline{OA}$ produced by other EAPs of the same size is 85.87%. Moreover, from the table one can see that the $EAP_{proposed}$ with 25 features provided an $\overline{OA}$ above 96%. Whereas, only few EAPs with 35 features constructed by the state-of-the-art method were able to obtain an $\overline{OA}$ of 96%. This confirms that the profile constructed by the proposed filtering method can incorporate sufficient spatial information during first few filtering operations. As a result, the proposed technique generates a smaller profile that not only incorporates sufficient spatial information but also avoids the curse of dimensionality problem and reduces the profile construction time.

The classification results obtained by considering different profiles for the CASI University of Houston data set are reported in Table III. Similarly to the previous results, also for this data set the $EAP_{proposed}$ outperformed than the EAPs constructed by the state-of-the-art method. Among all the considered increasing attributes and the non-increasing attribute *perimeter*, the $\overline{OA}$ produced by the $EAP_{proposed}$ with 15 features is above 94%. Whereas, the best EAP (EAP_{Num_pixel}) constructed by the state-of-the-art method could achieve a maximum of only 91.37% (considering the attribute *area*). This shows that the proposed technique exploits spatial information in much better way compared to the existing method. Moreover, from the table one can see that for the profiles created by the state-of-the-art method, the difference between the $\overline{OA}$ values obtained by the profiles of 15 and 25 features is more visible. Whereas, in case of the $EAP_{proposed}$ this difference is less relevant. This confirms that the proposed method is able to incorporate more spatial information during the first filtering operation.

From the above experiment one can see that the proposed filtering technique is effective for all the considered increasing attributes and also for the non-increasing attribute *perimeter*, which is close to the increasing behavior, whereas for the non-increasing attribute *Std* it produced similar results as the literature technique. Since *Std* is purely non-increasing in nature, starting from leaf to root node the LAF corresponding to a path will not be increasing and there may exist high fluctuations on the LAF. As a result, the generated MSC contains multiple local maxima. In this situation selecting the node that is associated with a global maximum in MSC may not be the best one for pruning. This is the reason for

TABLE III
CLASSIFICATION RESULTS OBTAINED FOR PROFILES CONSTRUCTED BY THE PROPOSED AND THE STATE-OF-THE-ART METHODS CONSIDERING FIVE DIFFERENT ATTRIBUTES (UNIVERSITY OF HOUSTON). THE BEST VALUES ARE HIGHLIGHTED IN BOLD FACE

		$EAP_{Num\_regions}$			EAP_{Num_pixel}			EAP_{Sum_gray}			$EAP_{proposed}$		
#features		15	25	35	15	25	35	15	25	35	15	25	35
Area	$\overline{OA}$	86.576	88.734	91.544	91.368	96.924	97.568	90.329	95.353	96.825	**95.684**	**96.970**	**97.793**
	kappa	0.8548	0.8782	0.9086	0.9067	0.9667	0.9737	0.8954	0.9498	0.9657	**0.9533**	**0.9672**	**0.9761**
	std	0.2963	0.3396	0.1882	0.2066	0.1874	**0.1863**	0.2029	0.2703	0.2830	**0.1742**	**0.1495**	0.1884
Perimeter	$\overline{OA}$	86.837	88.799	91.344	89.983	93.629	96.743	89.235	93.205	96.621	**94.582**	**95.993**	**97.169**
	kappa	0.8576	0.8789	0.9064	0.8917	0.9311	0.9648	0.8836	0.9265	0.9635	**0.9414**	**0.9567**	**0.9694**
	std	0.1580	0.2299	0.4229	**0.1410**	0.2501	0.1708	0.3684	0.2472	0.1681	0.1692	**0.1821**	**0.1566**
Abb	$\overline{OA}$	86.404	88.528	90.780	89.495	93.646	97.230	88.863	93.378	97.451	**95.163**	**96.951**	**97.838**
	kappa	0.8529	0.8759	0.9003	0.8864	0.9313	0.9701	0.8796	0.9284	0.9724	**0.9477**	**0.9670**	**0.9766**
	std	0.3673	0.2907	0.2003	0.2287	0.2802	0.2131	**0.2282**	0.1740	0.2108	0.3042	**0.1439**	**0.1511**
Dbb	OA	86.409	88.563	90.932	89.426	93.679	97.356	88.231	91.485	96.461	**94.103**	**97.140**	**97.742**
	kappa	0.8530	0.8763	0.9019	0.8857	0.9316	0.9714	0.8727	0.9079	0.9617	**0.9362**	**0.9691**	**0.9756**
	std	0.3811	**0.1815**	0.2598	0.3018	0.3395	**0.1580**	0.1837	0.2106	0.2470	**0.1676**	0.1905	0.1990
Std	OA	86.409	91.288	94.891	**91.990**	**95.056**	**95.854**	87.413	93.256	95.530	88.233	93.507	95.451
	kappa	0.8530	0.9058	0.9447	**0.9134**	**0.9465**	**0.9551**	0.8638	0.9270	0.9517	0.8727	0.9298	0.9508
	std	0.3811	0.2117	0.3947	**0.2270**	0.2271	0.2672	0.2569	**0.1581**	0.2047	0.3094	0.2333	**0.1480**

which the proposed technique produced lower accuracies for the *Std* attribute as compared to the other considered attributes. Nonetheless, it still provided similar results as those produced by the considered state-of-the-art method.

To further assess the effectiveness of the proposed method, the classification results obtained by using the proposed profiles ($EAP_{proposed}$) with 35 features are also compared to some recent spectral-spatial classification techniques such as EMEP, UNMIXING + SRC (referred as USRC), SRC, JSRC, MASR, SBSDM, SAS and CNN presented in [5]. The experiment is conducted on the CASI University of Houston data set considering the standard training and test set made available by the IEEE GRSS data fusion committee 2013. For this experiment, exactly the same experimental settings as used in [5] including the use of the random forest classifier with 200 trees are considered for classification of the constructed $EAP_{proposed}$. The classification results reported in Table IV show that the proposed technique outperforms many of the spectral-spatial classification techniques presented in [5]. This again shows the potentiality of proposed method for spectral-spatial classification of HSIs.

D. Results: Computational Time

In order to assess the effectiveness of the proposed technique in terms of computational time, Table V reports the times (in seconds) required by the proposed and the state-of-the-art method presented in [37] for the construction of different profiles having 35 features. Both the algorithms are implemented in MATLAB (R2015a) and tested on a workstation with Intel(R) Xeon(R) processor having 3.60 GHz processing power and 16 GB RAM. The time required for generating profiles $EAP_{Num\_regions}$, EAP_{Num_pixel}, EAP_{Sum_gray} and $EAP_{proposed}$ is denoted as T_{NR}, T_{NP}, T_{SG} and T_{prpsd}, respectively. From the table one can see that the proposed method can generate filtered images in an at least 50 times faster time than the state-of-the-art method. Moreover, for the *Std* attribute the proposed technique is extremely efficient in terms of computational time. Compared to the proposed technique, the technique presented in [37] requires more time because: (i) it creates GCF by evaluating a measure corresponding to a large number of possible threshold values; and (ii) it uses regression for approximating the GCF which requires a significant amount of time that is sensitive to the number of initial thresholds identified from the tree. On the other hand, the proposed filtering method has no such burden for threshold detection and the tree is filtered by applying only one depth first traversal.

TABLE V
COMPUTATIONAL TIME IN SECONDS REQUIRED FOR CONSTRUCTING SPECTRAL-SPATIAL PROFILES OF SIZE 35 USING THE STATE-OF-THE-ART METHOD AND THE PROPOSED METHOD

Data set	Attribute	T_{NR}	T_{NP}	T_{SG}	T_{prpsd}
University of Pavia	Area	3979	4148	4156	65
	Perimeter	2508	2490	2488	70
	Abb	3054	3143	3154	79
	Dbb	3636	3686	3646	80
	Std	795807	802349	816577	132
Indian Pines	Area	874	869	854	6
	Perimeter	519	521	528	6
	Abb	320	317	318	6
	Dbb	384	377	393	6
	Std	30859	31349	31442	44
University of Houston	Area	8068	8258	8253	368
	Perimeter	4240	4321	4316	339
	Abb	6282	6171	6175	371
	Dbb	7525	6181	7632	330
	Std	1097565	1007517	1087365	631

V. CONCLUSION

Attribute profiles for spectral-spatial classification existing in the literature detect threshold values either manually or automatically for generating the filtered images. Usually, since a single filtered image is unable to capture sufficient spatial information, multiple threshold values are used and several filtered images are generated. As a result, the construction of an attribute profile is time consuming and may result in a large number of features. To the best of our knowledge no method exists in the HSI literature that generate attribute profiles without employing threshold values. In this paper we have proposed a novel approach that generates the filtered

TABLE IV
OVERALL ACCURACY (OA), AVERAGE CLASSWISE-ACCURACY (AA) AND KAPPA COEFFICIENT (KAPPA) PROVIDED BY THE PROPOSED AND SEVERAL RECENT STATE-OF-THE-ART SPECTRAL-SPATIAL CLASSIFICATION METHODS USING STANDARD TRAINING AND TEST SETS. (UNIVERSITY OF HOUSTON DATA SET)

	Proposed Technique					Different Spectral-Spatial Techniques							
Accuracies	Area	Perimeter	Abb	Dbb	Std	EMEP	USRC	SRC	JSRC	MASR	SBSDM	SAS	CNN
OA	82.52	82.91	82.93	82.80	**82.95**	80.83	70.49	73.37	76.35	77.04	75.66	75.72	82.75
AA	**85.43**	85.33	85.30	85.23	85.38	83.64	77.25	78.35	78.35	79.74	78.26	78.08	84.04
kappa	0.8105	0.8149	0.8150	0.8136	**0.8152**	0.7920	0.6802	0.7128	0.7446	0.7520	0.7371	0.7376	0.8061

images for constructing attribute profiles without using the threshold values. The proposed filtering approach creates a tree to process connected components of the image and the insignificant objects are merged to their background objects. To this end, the path from the root to a leaf node is obtained using depth first traversal and a leaf attribute function (LAF) is defined to compute the attribute values of each node on the path. Then a novel criterion is defined to automatically detect the node on the path where the attribute values have first significant difference compared to its descendant nodes. Finally, all the descendants of the detected node are merged to it. The process is repeated for each path corresponding to the unvisited leaf nodes of the tree to generate the final filtered tree, which is transformed back to a filtered image. The proposed filtering method is repeated to generate multiple filtered images for constructing the attribute profiles.

In order to show the effectiveness of the proposed technique, the spectral-spatial profiles constructed by the proposed and a state-of-the-art method are compared on three hyperspectral images using five different attributes. The comparison showed that the proposed method has several advantages: (i) It generates filtered images without using any threshold value; (ii) It is fully automatic and independent on the image content; (iii) A small number of filtered images generated by this method are capable to capture a large amount of spatial information; (iv) It is more robust to handle curse of dimensionality problem; and (v) It generate the profiles in much faster way. Moreover, the proposed technique produces comparable classification results (some times better) with the different recent spectral-spatial classification techniques presented in the literature [5].

Although the proposed approach significantly reduced the computational time for profile generation, as a future work the proposed technique will be implemented in parallel processing environment to further increase its computational speed.

ACKNOWLEDGMENTS

The authors would like to thank the anonymous referees for their constructive criticism and valuable suggestions. The authors would also like to thank Dr. Saurabh Prasad, University of Houston for providing the Houston data set. This work is supported in part by a RPS-NER research grant from All India Council for Technical Education, New Delhi.

REFERENCES

[1] C.-I. Chang, *Hyperspectral data exploitation: theory and applications*. Hoboken, NJ, USA: John Wiley & Sons, 2007.

[2] H. J. Kramer, *Observation of the Earth and its Environment: Survey of Missions and Sensors*. New York, USA: Springer, 2002.

[3] F. Melgani and L. Bruzzone, "Classification of hyperspectral remote sensing images with support vector machines," *IEEE Transactions on geoscience and remote sensing*, vol. 42, no. 8, pp. 1778–1790, 2004.

[4] K. Bhardwaj and S. Patra, "An unsupervised technique for optimal feature selection in attribute profiles for spectral-spatial classification of hyperspectral images," *ISPRS Journal of Photogrammetry and Remote Sensing*, vol. 138, pp. 139–150, 2018.

[5] P. Ghamisi, E. Maggiori, S. Li, R. Souza, Y. Tarablaka, G. Moser, A. De Giorgi, L. Fang, Y. Chen, M. Chi *et al.*, "New frontiers in spectral-spatial hyperspectral image classification: The latest advances based on mathematical morphology, markov random fields, segmentation, sparse representation, and deep learning," *IEEE Geoscience and Remote Sensing Magazine*, vol. 6, no. 3, pp. 10–43, 2018.

[6] Y. Chen, N. M. Nasrabadi, and T. D. Tran, "Hyperspectral image classification using dictionary-based sparse representation," *IEEE transactions on geoscience and remote sensing*, vol. 49, no. 10, pp. 3973–3985, 2011.

[7] W. Fu, S. Li, L. Fang, X. Kang, and J. A. Benediktsson, "Hyperspectral image classification via shape-adaptive joint sparse representation," *IEEE Journal of Selected Topics in Applied Earth Observations and Remote Sensing*, vol. 9, no. 2, pp. 556–567, 2016.

[8] L. Fang, S. Li, X. Kang, and J. A. Benediktsson, "Spectral–spatial hyperspectral image classification via multiscale adaptive sparse representation," *IEEE Transactions on Geoscience and Remote Sensing*, vol. 52, no. 12, pp. 7738–7749, 2014.

[9] M.-D. Iordache, J. M. Bioucas-Dias, and A. Plaza, "Sparse unmixing of hyperspectral data," *IEEE Transactions on Geoscience and Remote Sensing*, vol. 49, no. 6, pp. 2014–2039, 2011.

[10] L. Fang, S. Li, X. Kang, and J. A. Benediktsson, "Spectral–spatial classification of hyperspectral images with a superpixel-based discriminative sparse model," *IEEE Transactions on Geoscience and Remote Sensing*, vol. 53, no. 8, pp. 4186–4201, 2015.

[11] Y. Chen, H. Jiang, C. Li, X. Jia, and P. Ghamisi, "Deep feature extraction and classification of hyperspectral images based on convolutional neural networks," *IEEE Transactions on Geoscience and Remote Sensing*, vol. 54, no. 10, pp. 6232–6251, 2016.

[12] S. Hao, W. Wang, Y. Ye, E. Li, and L. Bruzzone, "A deep network architecture for super-resolution-aided hyperspectral image classification with classwise loss," *IEEE Transactions on Geoscience and Remote Sensing*, vol. 56, no. 8, pp. 4650–4663, 2018.

[13] S. Hao, W. Wang, Y. Ye, T. Nie, and L. Bruzzone, "Two-stream deep architecture for hyperspectral image classification," *IEEE Transactions on Geoscience and Remote Sensing*, vol. 56, no. 4, pp. 2349–2361, 2018.

[14] J. A. Benediktsson, J. A. Palmason, and J. R. Sveinsson, "Classification of hyperspectral data from urban areas based on extended morphological profiles," *IEEE Transactions on Geoscience and Remote Sensing*, vol. 43, no. 3, pp. 480–491, 2005.

[15] J. Serra, *Image analysis and mathematical morphology*. London: Academic Press, 1982.

[16] J. Serra and L. Vincent, "An overview of morphological filtering," *Circuits, Systems, and Signal Processing*, vol. 11, no. 1, pp. 47–108, 1992.

[17] J. A. Benediktsson, M. Pesaresi, and K. Amason, "Classification and feature extraction for remote sensing images from urban areas based on morphological transformations," *IEEE Transactions on Geoscience and Remote Sensing*, vol. 41, no. 9, pp. 1940–1949, 2003.

[18] S. Patra, K. Bhardwaj, and L. Bruzzone, "A spectral-spatial multicriteria active learning technique for hyperspectral image classification," *IEEE Journal of Selected Topics in Applied Earth Observations and Remote Sensing*, vol. 10, no. 12, pp. 5213–5227, 2017.

[19] M. Dalla Mura, J. A. Benediktsson, B. Waske, and L. Bruzzone, "Morphological attribute profiles for the analysis of very high resolution images," *IEEE Transactions on Geoscience and Remote Sensing*, vol. 48, no. 10, pp. 3747–3762, 2010.

[20] L. Vincent, "Grayscale area openings and closings, their efficient implementation and applications," in *First Workshop on Mathematical Morphology and its Applications to Signal Processing*, 1993, pp. 22–27.

[21] E. J. Breen and R. Jones, "Attribute openings, thinnings, and granulometries," *Computer Vision and Image Understanding*, vol. 64, no. 3, pp. 377–389, 1996.

[22] P. Salembier, A. Oliveras, and L. Garrido, "Antiextensive connected operators for image and sequence processing," *IEEE Transactions on Image Processing*, vol. 7, no. 4, pp. 555–570, 1998.

[23] B. Song, J. Li, M. Dalla Mura, P. Li, A. Plaza, J. M. Bioucas-Dias, J. A. Benediktsson, and J. Chanussot, "Remotely sensed image classification using sparse representations of morphological attribute profiles," *IEEE transactions on geoscience and remote sensing*, vol. 52, no. 8, pp. 5122–5136, 2014.

[24] J. Xia, M. Dalla Mura, J. Chanussot, P. Du, and X. He, "Random subspace ensembles for hyperspectral image classification with extended morphological attribute profiles," *IEEE Transactions on Geoscience and Remote Sensing*, vol. 53, no. 9, pp. 4768–4786, 2015.

[25] B. Demir and L. Bruzzone, "Histogram-based attribute profiles for classification of very high resolution remote sensing images," *IEEE Transactions on Geoscience and Remote Sensing*, vol. 54, no. 4, pp. 2096–2107, 2016.

[26] Z. Zhang and M. M. Crawford, "A batch-mode regularized multimetric active learning framework for classification of hyperspectral images," *IEEE Transactions on Geoscience and Remote Sensing*, vol. 55, no. 11, pp. 6594 – 6609, 2017.

[27] A. Das, K. Bhardwaj, and S. Patra, "Morphological complexity profile for the analysis of hyperspectral images," in *2018 4th International Conference on Recent Advances in Information Technology (RAIT)*. IEEE, 2018, pp. 1–6.

[28] M. Dalla Mura, J. A. Benediktsson, B. Waske, and L. Bruzzone, "Extended profiles with morphological attribute filters for the analysis of hyperspectral data," *International Journal of Remote Sensing*, vol. 31, no. 22, pp. 5975–5991, 2010.

[29] P. R. Marpu, M. Pedergnana, M. Dalla Mura, S. Peeters, J. A. Benediktsson, and L. Bruzzone, "Classification of hyperspectral data using extended attribute profiles based on supervised and unsupervised feature extraction techniques," *International Journal of Image and Data Fusion*, vol. 3, no. 3, pp. 269–298, 2012.

[30] P. Ghamisi, J. A. Benediktsson, and J. R. Sveinsson, "Automatic spectral–spatial classification framework based on attribute profiles and supervised feature extraction," *IEEE Transactions on Geoscience and Remote Sensing*, vol. 52, no. 9, pp. 5771–5782, 2014.

[31] P. Ghamisi, M. Dalla Mura, and J. A. Benediktsson, "A survey on spectral–spatial classification techniques based on attribute profiles," *IEEE Transactions on Geoscience and Remote Sensing*, vol. 53, no. 5, pp. 2335–2353, 2015.

[32] G. Hughes, "On the mean accuracy of statistical pattern recognizers," *IEEE transactions on information theory*, vol. 14, no. 1, pp. 55–63, 1968.

[33] M. Pedergnana, P. R. Marpu, M. Dalla Mura, J. A. Benediktsson, and L. Bruzzone, "A novel technique for optimal feature selection in attribute profiles based on genetic algorithms," *IEEE Transactions on Geoscience and Remote Sensing*, vol. 51, no. 6, pp. 3514–3528, 2013.

[34] N. Falco, J. A. Benediktsson, and L. Bruzzone, "Spectral and spatial classification of hyperspectral images based on ICA and reduced morphological attribute profiles," *IEEE Transactions on Geoscience and Remote Sensing*, vol. 53, no. 11, pp. 6223–6240, 2015.

[35] Z. Mahmood, G. Thoonen, and P. Scheunders, "Automatic threshold selection for morphological attribute profiles," in *Geoscience and Remote Sensing Symposium (IGARSS), 2012 IEEE International*. IEEE, 2012, pp. 4946–4949.

[36] P. R. Marpu, M. Pedergnana, M. Dalla Mura, J. A. Benediktsson, and L. Bruzzone, "Automatic generation of standard deviation attribute profiles for spectral–spatial classification of remote sensing data," *IEEE Geoscience and Remote Sensing Letters*, vol. 10, no. 2, pp. 293–297, 2013.

[37] G. Cavallaro, N. Falco, M. Dalla Mura, and J. A. Benediktsson, "Automatic attribute profiles," *IEEE Transactions on Image Processing*, vol. 26, no. 4, pp. 1859–1872, 2017.

[38] E. Carlinet and T. Géraud, "A comparative review of component tree computation algorithms," *IEEE Transactions on Image Processing*, vol. 23, no. 9, pp. 3885–3895, 2014.

[39] P. Bosilj, E. Kijak, and S. Lefèvre, "Partition and inclusion hierarchies of images: A comprehensive survey," *Journal of Imaging*, vol. 4, no. 2, p. 33, 2018.

[40] L. Najman and M. Couprie, "Building the component tree in quasi-linear time," *IEEE Transactions on image processing*, vol. 15, no. 11, pp. 3531–3539, 2006.

[41] C.-C. Chang and C.-J. Lin, "LIBSVM: a library for support vector machines," *ACM Transactions on Intelligent Systems and Technology (TIST)*, vol. 2, no. 3, p. 27, 2011.

[42] D. Lemire, "A better alternative to piecewise linear time series segmentation," in *Proceedings of the 2007 SIAM International Conference on Data Mining*. SIAM, 2007, pp. 545–550.